Interface Reconstruction Study by Functional Scanning Probe Microscope in Li-ion Battery Research①

JIA Lang-Lang# JI Yu-Chen# YANG Kai
WANG Zi-Jian CHEN Hai-Biao② PAN Feng②
(*School of Advanced Materials, Peking University Shenzhen Graduate School, Shenzhen* 518055, *China*)

ABSTRACT Interfacial reaction is a critical factor of lithium ion battery, but is also complicated and difficult to characterize. Scanning probe microscope (SPM) is one of the most effective tools to reveal the interface reconstruction and interfacial properties (including the morphologies, mechanical properties and electricity properties) of energy material at nanoscale and at real time. In this paper, we briefly summarized the principles of AFM, conductive AFM(C-AFM) and Kelvin probe force microscope (KPFM), as well as their application to investigate the interface reconstruction of lithium-ion battery electrode material.

Keywords: SPM, AFM, KPFM, C-AFM, battery; DOI: 10.14102/j.cnki.0254–5861.2011–2749

1 INTRODUCTION

With the rapid development of clean energy industry, lithium ion batteries (LIBs) have become an important technology for electric energy storage owing to their high energy density and stable cycling performance[1]. Understanding the fundamental mechanisms in electrode-electrolyte reaction and electrode degradation is critical for the improvement of battery performance. In the past decades, various *ex-situ* and *in-situ* characterization tools have been developed to investigate the interfacial reaction mechanisms and structure evolutions of electrode materials[2]. Scanning probe microscope (SPM) is a collection of tools to characterize phenomena and properties at the nanoscale by detecting various interactions between a probe tip and the sample. Different types of SPM have been developed, such as electrochemical atomic force microscope (EC-AFM), conductive AFM (C-AFM), electrochemical strain microscope (ESM) and Kelvin probe force microscope (KPFM)[3]. In recent years, SPMs have been demonstrated as powerful tools with a unique capability for directly visualizing the static and dynamic morphology of the surface of the electrodes during typical electrochemical processes[4]. This perspective focuses on the application of *ex-situ* and *in-situ* functional SPM techniques in battery researches.

2 OPERATION PRINCIPLES OF DIFFERENT SPMs

As the most popular type of SPM, AFM was first invented in 1986[5] and now has become an important tool for surface characterization down to the atomic scale. SPM including AFM is operated based on the principle that as a solid probe is brought close enough

Received 26 January 2020; accepted 2 February 2020
① This work was supported by the National Key R&D Program of China (2016YFB0700600), Soft Science Research Project of Guangdong Province (No. 2017B030301013), and Shenzhen Science and Technology Research Grant (ZDSYS201707281026184)
② Corresponding authors. E-mails: panfeng@pkusz.edu.cn and E-mail: chenhb@pkusz.edu.cn
#These authors contributed equally to this work

to the sample surface the interaction force can be sensed by a detector. Depending on the analysis, the interaction of interest can be short-range repulsive force, or long-range interactions including van der Waals forces, magnetic and electrostatic interactions[6]. Based on the type of interactions, SPMs operating in different modes have been developed. For example, surface morphology, surface roughness, mechanical properties (stiffness, adhesiveness, viscosity) and electrical properties (work function, surface potential and conductivity) are commonly analyzed by SPMs[3]. Table 1 lists different types of SPM systems and their capabilities. Usually, a typical functional SPM can simultaneously measure multiple physicochemical and electrical properties with a nanoscale resolution.

Table 1. Summary of Different SPM Systems

Technique	Interaction	Substrate	Measurement
AFM	Repulsive force	No special requirements	Morphology, roughness, stiffness
C-AFM	Repulsive force	Conductive	Current distribution
KPFM	Electrostatic interactions	Conductive	Work function
EFM	Electrostatic interactions	Solid	Local electrochemical activity
SICM, SECM, SECCM	Electrostatic interactions	Liquid	Topography and conductivity

*AFM (atomic force microscopy), C-AFM (conductive AFM), KPFM (Kelvin probe force microscopy), EFM (electrostatic force microscopy), SICM (scanning ion conductance microscopy), SECM (scanning electrochemical microscopy), and SECCM (scanning electrochemical cell microscopy)

3 CHARACTERIZATION OF MORPHOLOGY AND MECHANICAL PROPERTIES

The most commonly utilized function of an AFM is to visualize the surface morphology of a solid. For LIBs, the surface of an electrode is in direct contact with the electrolyte and experiences complex physical and chemical changes during typical char-ging and discharging of the battery. As a key element in LIBs, electrolyte can largely determine the performance of the battery. The electrolyte can decompose during an electrochemical process and the products depositing on the electrode surface form a solid-electrolyte interface (SEI) layer. The evolution of the surface of an electrode during an electro-chemical process can be visualized using a specially designed AFM cell. As shown in Fig. 1a, Lin et al. employed the *in-situ* AFM to observe the effect of sulfur-containing additives on the formation process of the SEI layer on highly oriented pyrolytic graphite (HOPG). The surface morphology of the SEI layer was monitored in real time during a cyclic voltammetry (CV) scan. Ethylene sulfite additive was found to be reduced to form the initial SEI at a relatively higher potential and then transformed to a more stable and denser SEI layer to protect the surface of the graphite electrode[7]. Liu et al. studied the detailed process of SEI formation in an ethylene carbonate (EC) electrolyte by combining *in-situ* AFM, EQCM (Electrochemical Quartz Crystal Micro-balance), and DEMS (Differential Electro-chemical Mass Spectrometry)[8], as shown in Fig. 1c. During a potential sweeping, the formation of the components in the SEI layer could be divided into five consecutive and distinct stages: (1) LiF formation at 1.5 V, (2) co-intercalation of $Li^+(solvent)_x$ at 0.88 V, (3) initial EC reduction at 0.74 V, (4-5) major EC reduction at lower potentials, and (6) lithium alkyl carbonates produced by re-oxidation of partially reduced EC during anodic scan above 0.3 V. While many *in-situ* AFM studies focus on LIBs, Yang et al. employed *in-situ* AFM to analyze the intercalation process in dual ion batteries (DIBs)[9]. By measuring the change in the distance between the graphene layers during anion (PF_6^-) intercalation, they found that PF_6^- intercalated in one of every three graphite layers and the anion intercalation speed was 0.2 μm·min^{-1}. The nano-mechanical properties of the electrodes in LIBs can be also studied by AFM. Xu et al. employed an AFM nano-indentation technique to measure the

stiffness of the SEI layer formed on Si nanowires[10]. Zhang et al. reported quantitative measurement of the modulus of SEI films on MnO anodes[11], as depicted in Fig. 1b. By measuring the SEI thickness and Young's modulus, they found that SEI layers formed under different potentials showed different mechanical properties such as stiffness and multi-layer structures.

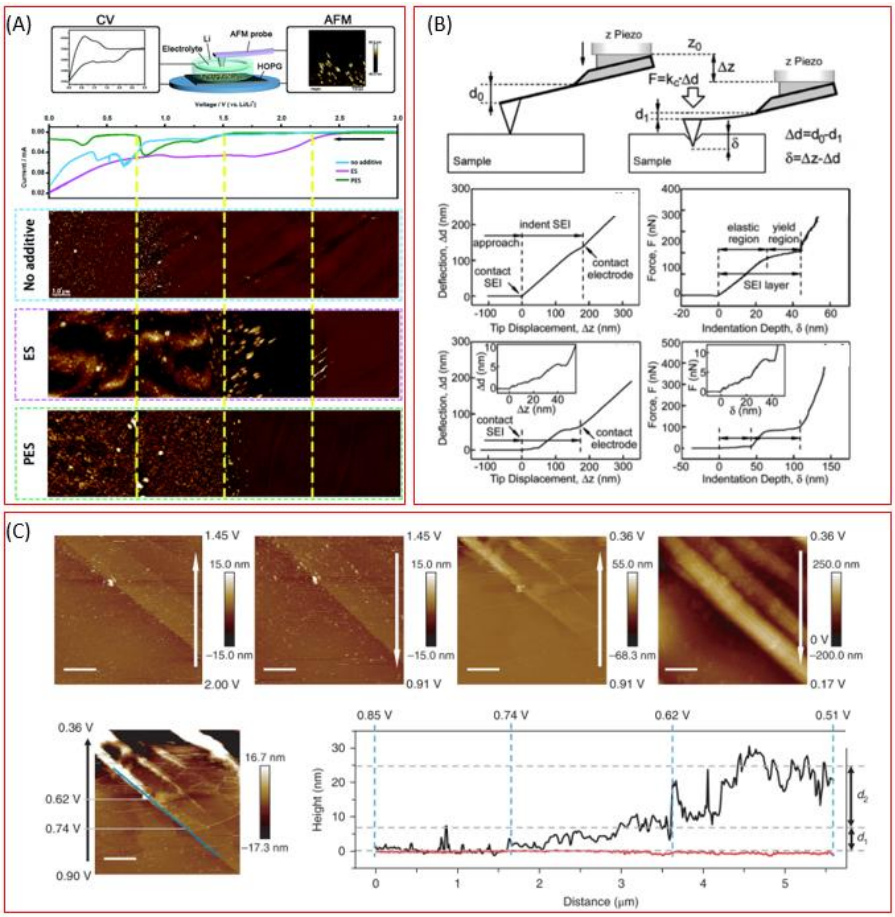

Fig. 1. Morphology and mechanical properties characterization of energy materials. (A) *In-situ* AFM observation of sulfur-contained additives effect on the SEI formation process on HOPG. Reproduced with permission from Ref[7]. (B) Mechanical properties of SEI films on MnO anodes measured by AFM. Reproduced with permission from Ref[11]. (C) *In-situ* quantification of SEI formation on graphite anode in carbonate electrolyte. Reproduced with permission from Ref[8]

4 CHARACTERIZATION OF ELECTRICAL PROPERTIES

Another important information that can be accessed by SPM is the electrical properties of an electrode. During the charging and discharging processes, the insertion/de-insertion of lithium ions could cause the phase transformation and changes in the electrical properties of the electrode materials. The changes in these electrical properties (such as conductivity and surface potential) can be detected by SPM systems.

C-AFM is also known as current sensing-AFM. By applying a bias voltage between the probe and the sample, the micro-zone current in the closed loop circuit can be detected and it represents the conductive properties. Huang et al. employed *in-situ* peak force tunneling AFM (PF-TUNA) to reveal the phase transformation of $LiCoO_2$ during the charging process[12] (Fig. 2a). Under different potentials, the deintercalation of lithium ions caused the change of current distribution on the Li_xCoO_2 surface, which reveals the phase transformation of the electrode material from O3-I to O3-Ⅱ phase. Meng studied

the lithiation process of $Li_4Ti_5O_{12}$ by C-AFM[13], as shown in Fig. 2c. While there is no obvious morphology difference between $Li_4Ti_5O_{12}$ and $Li_7Ti_5O_{12}$, C-AFM could distinguish the $Li_4Ti_5O_{12}$ (insulator) and $Li_7Ti_5O_{12}$ (conductor) by measuring the conductivity. Lee et al. observed the anisotropic conductivity of a single crystal of Li_xCoO_2 during the charging process by C-AFM[14] (Fig. 2b**)**. With the help of SEM, the AFM tip can precisely engage on the surface perpendicular or parallel to the (003) lattice plane, and the conductivity on this plane was found to be higher than that on other planes.

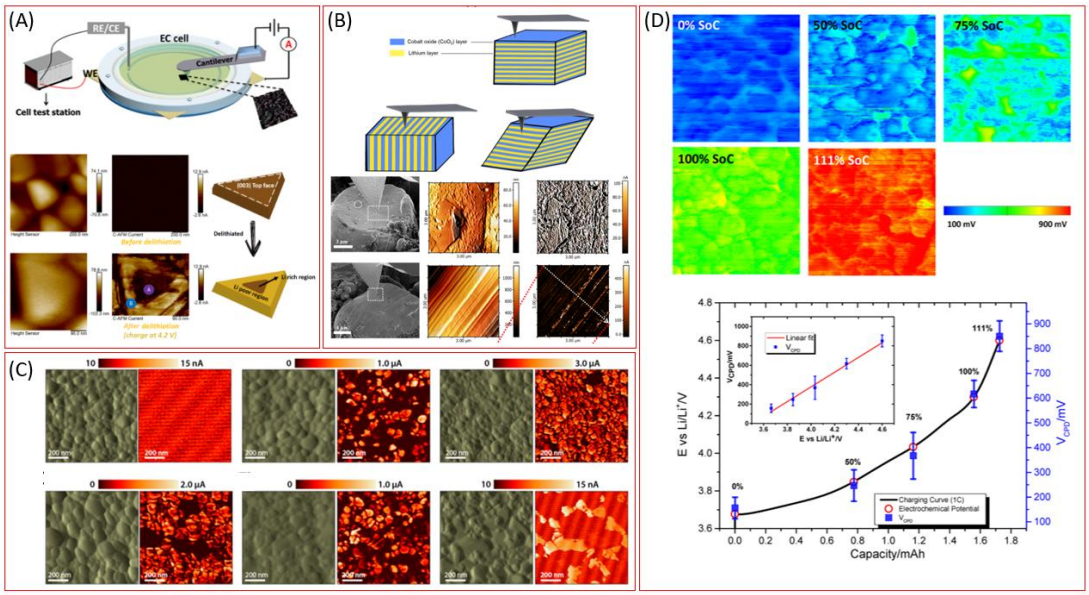

Fig. 2. Electrical properties characterization of energy materials. (A) *In-situ* C-AFM revealed the non-equilibrium phase transformation of $LiCoO_2$ cathode material during the charging process. Reproduced with permission from Ref[12]. (B) SEM assisted AFM observation of conductivity on different crystal planes of $LiCoO_2$. Reproduced with permission from Ref[14]. (C) Conductivity evolution of $Li_4Ti_5O_{12}$ in different states of lithiation measured by C-AFM. Reproduced with permission from Ref[13]. (D) Correlation between the surface and electrochemical potentials of $LiNi_{0.80}Co_{0.15}Al_{0.05}O_2$ cathode. Reproduced with permission from Ref[15]

The Kelvin probe force microscopy (KPFM) can directly measure the surface potential between the sample and AFM tip[16]. The surface potential can also be called the contact potential difference (CPD) and is defined as:

$$V_{CPD} = \frac{\varphi_{tip} - \varphi_{sample}}{e} \quad (1)$$

The φ_{tip} and φ_{sample} are the work functions of the tip and the sample, respectively, and e represents the unit electronic charge. The work function is an intrinsic property of material and presents the difference between the vacuum energy level (E_V) and the Fermi energy level (E_F):

$$\varphi = E_V - E_F \quad (2)$$

Kholkin et al. used KPFM to detect the distribution of lithium ions in aged graphite anodes at high current densities[17]. The surface potential of the lithiated graphite decreased in comparison to the blank graphite. By measuring the surface potential distri-bution of the aged graphite, they found that the Li^+ ions were trapped in graphite particles especially under a high current density, which caused the capacity decay. Babu et al. compared the surface potential of aged and pristine $LiFePO_4$ cathode, and found that the phase change, nanoparticle coarsening, and loss of carbon coating can subtly change the surface potential of the material[18]. Hubin et al. used KPFM to reveal correlation between the surface and electrochemical potentials of $LiNi_{0.80}Co_{0.15}Al_{0.05}O_2$ cathode material[15], as depicted in Fig. 2d. The surface potential of the electrode at different states of charge was measured by KPFM, and the result

presented that the surface potential was positively correlated to the charge potential, which can also be related to the state of charge. Masuda combined *in-situ* cross-sectional KPFM with Ar ion milling to directly image the internal potential distribution of cathode electrode in an all-solid-state Li ion battery[19]. The distribution and the conductive path of lithium ions can be visualized in real time. Zeng et al. directly used the tip of KPFM probe as an anodic current collector to transport electrons and simultaneously detect the surface potential[20]. The distribution and change of surface potential on the polycrystalline TiO_2 anode film at different biasing conditions were clearly observed. The slight decrease of surface potential will cause the decrease of conductivity and capacity decay of TiO_2 anode.

5 OUTLOOK

SPM techniques have been widely used in lithium-ion battery research. Benefiting from the develop-ment of SPM techniques, topographic, mechanical, and electrochemical properties of materials in LIBs can be observed and measured quantitively in real time and at nanoscale utilizing various functional imaging modes. We pose that the SPM techniques can be further developed in the following directions: (1) SPM systems can be integrated with other charac-terization techniques especially *in-situ* chemical analysis systems such as Raman, FTIR and EDS mapping to provide more information on the com-positional and structural evolutions. (2) Many AFM studies of LIBs employed an idealized electrode material l HOPG as the substrate instead of real-life electrodes to ensure reliable measurement. It is still challenging to apply AFM characterizations to real-life electrodes. In this regard, special sample preparation methods including magnetron sputtering, FIB milling, CVD and PVD to prepare a smooth sample surface should be developed. (3) Many other interfacial reactions and structure evolution in energy materials can be investigated: such as lithium dendrite growth and ion diffusion in solid-state-battery, multi-valent ions (Al^{3+}, Mg^{2+}, Ca^{2+}) intercalation behavior in layered materials, surface and structure reconstruc-tion in high voltage cathode materials (Li-rich and high nickle cathode).

REFERENCES

(1) Lu, J.; Chen, Z.; Pan, F.; Cui, Y.; Amine, K. High-performance anode materials for rechargeable lithium-ion batteries. *Electrochem. Energy Rev.* **2018**, 1, 35–53.

(2) Hui, J.; Gossage, Z. T.; Sarbapalli, D.; Hernández-Burgos, K.; Rodríguez-López, J. Advanced electrochemical analysis for energy storage interfaces. *Anal. Chem.* **2019**, 91, 60–83.

(3) Chen, X.; Lai, J.; Shen, Y.; Chen, Q.; Chen, L. Functional scanning force microscopy for energy nanodevices. *Adv. Mater.* **201**8, 30, 1802490.

(4) Wang, S.; Liu, Q.; Zhao, C.; Lv, F.; Qin, X.; Du, H.; Kang, F.; Li, B. Advances in understanding materials for rechargeable lithium batteries by atomic forcemicroscopy. *Energy Environ. Mat.* **2018**, 1, 28–40.

(5) Binnig, G.; Rohrer, H.; Gerber, C.; Weibel, E. 7×7 Reconstruction on Si(111) resolved in real space. *Phys. Rev. Lett.* **1983**, 50, 120–123.

(6) Kalinin, S. V.; Dyck, O.; Balke, N.; Neumayer, S.; Tsai, W. Y.; Vasudevan, R.; Lingerfelt, D.; Ahmadi, M.; Ziatdinov, M.; McDowell, M. T.; Strelcov, E. Toward electrochemical studies on the nanometer and atomic scales: progress, challenges, and opportunities. *ACS Nano.* **2019**, 13, 9735−9780.

(7) Lin, L.; Yang, K.; Tan, R.; Li, M.; Fu, S.; Liu, T.; Chen, H.; Pan, F. Effect of sulfur-containing additives on the formation of a solid-electrolyte interphase evaluated by *in situ* AFM and ex situ characterizations. *J. Mater. Chem. A* **2017**, 5, 19364−19370.

(8) Liu, T.; Lin, L.; Bi, X.; Tian, L.; Yang, K.; Liu, J.; Li, M.; Chen, Z.; Lu, J.; Amine, K.; Xu, K.; Pan, F. *In situ* quantification of interphasial chemistry in Li-ion battery. *Nat. Nanotechnol.* **2019**, 14, 50–60.

(9) Yang, K.; Jia, L.; Liu, X.; Wang, Z.; Wang, Y.; Li, Y.; Chen, H.; Wu, B.; Yang, L.; Pan, F. Revealing the anion intercalation behavior and surface evolution of graphite in dual-ion batteries via in situ AFM. *Nano. Res.* **2020**.

(10) Xu, W.; Vegunta, S. S. S.; Flake, J. C. Surface-modified silicon nanowire anodes for lithium-ion batteries. *J. Power Sources* **2011**, 196, 8583–8589.

(11) Zhang, J.; Wang, R.; Yang, X. C.; Lu, W.; Wu, X. D.; Wang, X. P.; Li, H.; Chen, L. W. Direct observation of inhomogeneous solid electrolyte

interphase on MnO anode with atomic force microscopy and spectroscopy. *Nano. Letters* **2012**, 12, 2153−2157.

(12) Chen, Y.; Yu, Q.; Xu, G.; Zhao, G.; Li, J.; Hong, Z.; Lin, Y.; Dong, C. L.; Huang, Z. Chen, Y.; Yu, Q.; Xu, G.; Zhao, G.; Li, J.; Hong, Z.; Lin, Y.; Dong, C. L.; Huang, Z. *In situ* observation of the insulator-to-metal transition and nonequilibrium phase transition for $Li_{1-x}CoO_2$ films with preferred (003) orientation nanorods. *ACS Appl. Mater. Interfaces* **2019**, 11, 33043−33053

(13) Verde, M. G.; Baggetto, L.; Balke, N.; Veith, G. M.; Seo, J. K.; Wang, Z.; Meng, Y. S. Elucidating the phase transformation of $Li_4T_{i5}O_{12}$ lithiation at the nanoscale. *ACS Nano.* **2016**, 10, 4312−4321.

(14) Kang, H.; Lee, J.; Rodgers, T.; Shim, J. H.; Lee, S. Electrical conductivity of delithiated lithium cobalt oxides: conductive atomic force microscopy and density functional theory study. *J. Phys. Chem. C* **2019**, 123, 17703−17710.

(15) Zhu, X.; Revilla, R. I.; Hubin, A. Direct correlation between local surface potential measured by Kelvin probe force microscope and electrochemical potential of $LiNi_{0.80}Co_{0.15}Al_{0.05}O_2$ cathode at different state of charge. *J. Phys. Chem. C* **2018**, 122, 28556−28563.

(16) Jacobs, H. O.; Leuchtmann, P.; Homan, O. J.; Stemmer, A. Resolution and contrast in Kelvin probe force microscopy. *J. Appl. Phys.* **1998**, 84, 1168−1173.

(17) Luchkin, S. Y.; Amanieu, H. Y.; Rosato, D.; Kholkin, A. L. Li distribution in graphite anodes: a Kelvin probe force microscopy approach. *J. Power Sources* **2014**, 268, 887−894.

(18) Nagpure, S. C.; Bhushan, B.; Babu, S. S. Surface potential measurement of aged Li-ion batteries using Kelvin probe microscopy. *J. Power Sources* **2011**, 196, 1508−1512.

(19) Masuda, H.; Ishida, N.; Ogata, Y.; Ito, D.; Fujita, D. Internal potential mapping of charged solid-state-lithium ion batteries using in situ Kelvin probe force microscopy. *Nanoscale* **2017**, 9, 893−898.

(20) Zhu, J.; Zeng, K.; Lu, L. *In-situ* nanoscale mapping of surface potential in all-solid-state thin film Li-ion battery using Kelvin probe force microscopy. *J. Appl. Phys.* **2012**, 111, 1−7.